15th ISA Aerospace Instrumentation Symposium, May 1968; also AEDC TR-69-182, 1969, Arnold Engineering Development Center, Arnold Air Force Station, Tullahoma, Tenn.

[10] Martellucci, A., "Effects of Mass Transfer on Hypersonic Turbulent Boundary-Layer Properties," *AIAA Journal*, Vol. 10, No. 2, Feb. 1972, pp. 181–187.

[11] Johnson, C. B. and Bushnell, D. M., "Power-Law Velocity Profile and Mach Number in a Turbulent Boundary Layer," TND-5753, April 1970, NASA.

[12] Lowson, M. V., "Predictions of Boundary Layer Pressure Fluctuations," AFFDL-TR-67-167, April, 1968, Air Force Flight Dynamics Lab., Wright-Patterson Air Force Base, Ohio.

[13] Houbolt, J. C., "On the Estimation of Pressure Fluctuations in Boundary Layers and Wakes," GE-TIS 66SD296, Aug. 1966, General Electric Co., Philadelphia, Pa.

[14] Owen, F. K. and Horstman, C. C., "Hypersonic Transitional Boundary Layers," *AIAA Journal*, Vol. 10, No. 6, June 1972, pp. 769–775.

[15] Donaldson, J. C. and Wallace, J. P., "Flow Fluctuations Measurements at Mach Number 4 in the Test Section of the 12-Inch Supersonic Tunnel," AEDC-TR-71-143, Aug. 1971, Arnold Engineering Development Center, Arnold Air Force Base, Tullahoma, Tenn.

[16] Kendall, J. M., Jr., "Supersonic Boundary Layer Transition Studies," *Space Programs Summary 37–62*, Vol. III, J. P. L. Propulsion Lab., Pasadena, Calif., 1970.

[17] Kendall, J. M., Jr., "J. P. L. Experimental Investigations," *Proceedings of the Boundary Layer Transition Workshop*, SAMSO-Dec. 1971, pp. 2-1 to 2-16.

[18] Mack, L. M., "Progress in Compressible Boundary Layer Stability Computations," *Proceedings of the Boundary Layer Transition Workshop*, Aerospace Corp., Dec. 1971, pp. 1-1 to 1-35.

[19] Fischer, M. C. and Weinstein, L. M., "Come Transitional Boundary-Layer Structure at $M_e = 14$," *AIAA Journal*, Vol. 10, No. 5, May 1972, pp. 699–701.

[20] Stainback, P. C., "Use of Rouse's Stability Parameter in Determining the Critical Layer Height of a Laminar Boundary Layer," *AIAA Journal*, Vol. 8, No. 1, Jan. 1970, pp. 173–175.

MAY 1973 AIAA JOURNAL VOL. 11, NO. 5

Aerodynamics of High-Performance Ludwieg Tubes

DAVID A. RUSSELL* AND KWOK-ON TONG†
University of Washington, Seattle, Wash.

A small perturbation analysis of the flow in a Ludwieg tube supply is described which includes both the growing turbulent boundary layer and pipe axial nonuniformities. Measured pressure time histories are used to check the theory and its extension to high pipe Mach numbers and large flow perturbations. The nonsteady coupling of this flow to a nozzle is investigated. Calculations are made of the effects on the nozzle boundary layer, while a separate analysis is carried out for the case of complete mixing in a nozzle plenum. The double expansion nozzle is shown to extend Ludwieg tube capability. Analytical and experimental studies are made of aerodynamic problems that can arise in these nozzles.

Nomenclature

A = geometric cross-sectional area (refers to test section unless otherwise indicated)
a = speed of sound
D = orifice plate hole spacing
d = pipe diameter
L = supply tube length
M = flow Mach number (refers to test section unless otherwise indicated)
p = static pressure
Re = Reynolds number of test flow (based on suitable length)
s = wave fixed coordinate (Figs. 2 and 3)
T = static temperature
t = time
U = single speed assigned to expansion wave (equal to a_4 for small M_3)
u = flow velocity in axial direction
V = staged nozzle volume between A_{op}* and A*
x = coordinate in axial direction
γ = ratio of specific heats
Δ = perturbation
δ* = boundary-layer displacement thickness (given by Fig. 2)
δ_s* = boundary-layer displacement thickness in wave fixed coordinates (equal to $M_3\delta$* for Becker model at small M_3)
ε = boundary-layer total energy thickness
θ = boundary-layer momentum thickness
ρ = static density

Subscripts
e = core flow value (radial variations neglected)
eff = effective value (including boundary-layer effects)
o = stagnation value (refers to test section unless otherwise indicated)
op = orifice plate value
p = plenum exit value
rms = root-mean-square of fluctuation
3 = unperturbed flow behind expansion wave
4 = initial conditions in the supply

Superscript
* = throat value (refers to test section unless otherwise indicated)

Presented as Paper 72-994 at the AIAA 7th Aerodynamic Testing Conference, Palo Alto, Calif., September 13–15, 1972; submitted September 25, 1972; revision received December 26, 1972. This work was supported by NASA Grant NGR 48-002-107. The authors would like to acknowledge valuable contributions from V. Buonadonna, C. Padova, L. J. Runyan, and J. Wai. The starting time of double nozzles was worked out in collaboration with T. G. Jones of Mathematical Sciences Northwest Inc.

Index categories: Aircraft and Component Wind Tunnel Testing; Nozzle and Channel Flow; Boundary Layers and Convective Heat Transfer—Turbulent.

* Associate Professor, Department of Aeronautics & Astronautics. Associate Fellow AIAA.

† Graduate Student, Department of Aeronautics & Astronautics.

Introduction

LUDWIEG tubes offer a convenient way of producing high-mass-flux aerodynamic test flows. As shown on the upper sketch of Fig. 1, a Ludwieg tube consists essentially of a long

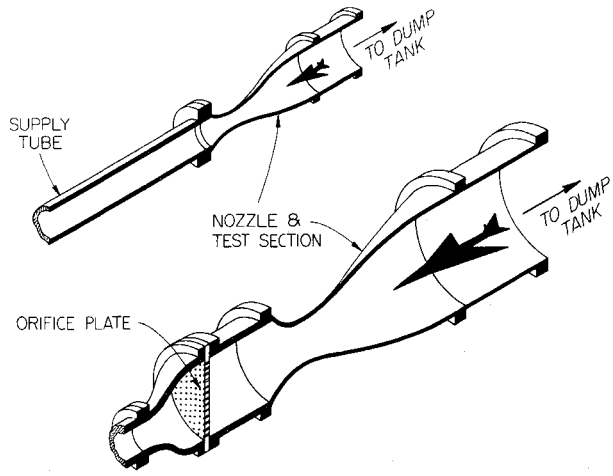

Fig. 1 Schematic Ludwieg tubes with conventional and double expansion nozzles.

pressurized pipe connected to a nozzle. A diaphragm or quick-opening valve initiates the flow, which is maintained until the leading edge of the pipe expansion wave has returned from the closed end. Since Ludwieg's original work in 1955,[1] studies have outlined the general performance and design features of this type of wind tunnel.[2] Many small facilities have been constructed, and there are now plans to use large Ludwieg tubes for full flight Reynolds number simulation.[2,3] Ludwieg tubes are generally conceived of as producing very high quality test flows. The degree to which this is true is the subject of the present paper, which considers both conventional Ludwieg tubes and those designed to maximize useful Re capability.

A major source of test flow perturbation is the nonsteady turbulent boundary layer in the supply pipe. In general the thickness of this boundary layer depends on the distance behind the expansion wave, the wave thickness, the initial pressure and temperature of the supply gas, and the nominal pipe Mach number. It is convenient to introduce the pipe diameter and to express δ^*/d in terms of the instantaneous aspect ratio of the flow (s/d), p_4d, M_3, and some measure of the wave thickness or of its origin. The results from two different models for δ^*/d are shown on Fig. 2, evaluated for nitrogen with $T_4 = 300°K$. Both analyses assume a $\frac{1}{7}$th power law for the velocity profile and a zero-thickness expansion wave. However, Mirels[4] measures s from the head of the actual wave while Becker[5] uses a weighted position within it. The simplified Becker model further

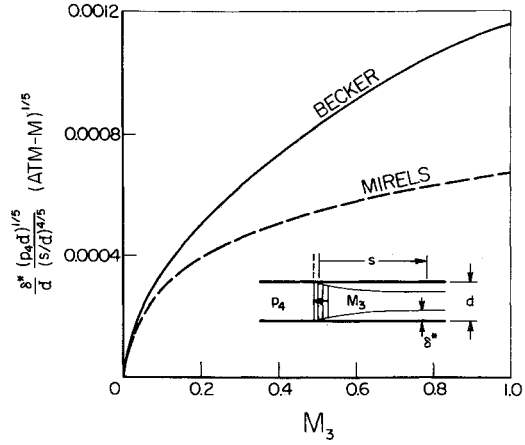

Fig. 2 Turbulent boundary-layer displacement thickness behind zero thickness expansion wave.

assumes that the density is constant across the boundary layer, while Mirels uses a polynomial form for the temperature profile. As might be expected, the model predictions are seen to be in agreement for weak expansion waves (low M_3), but diverge at high M_3 where neither model can be correct. Regardless of the model used, Fig. 2 will show that at the end of the test time ($s \approx 2L$) the thickness of the boundary layer ($\approx 10\delta^*$) at the exit of a typical Ludwieg tube supply approaches the pipe radius.

The consequences of this boundary layer are carefully explored in the present study. A linearized analysis of the effect on the pipe core flow is discussed which is felt to be more direct and consistent than Becker's original treatment of this phenomena,[6] although the Becker boundary-layer model[5] (Fig. 2) is used for simplicity. Experiments are used to check the results and to guide use of the predictions at high M_3. The analysis is extended to include the important influences of cross-sectional area and wall temperature variation along the pipe. Attention then shifts to following the exit flow from the supply pipe into the test nozzle. Steady boundary-layer calculations are made along a series of assumed nozzle wall contours, using the growing pipe exit δ^* of Fig. 2 as the starting point. The results show the importance of the nozzle entrance contraction ratio (low M_3) for suppressing nonsteady flow in the test section. The pipe exit boundary layer and core flow may be effectively stagnated and mixed in a nozzle plenum. This is discussed with the aid of a simple linearized mixing analysis.

The various studies are kept as general as possible so that they may be applied to any Ludwieg tube configuration. The limited strength of aerodynamic models restricts pressure levels, resulting in a need for large test section dimension if Re simulation is sought. This may be realized through an increase in facility scale, by opening up the throat of a conventional Ludwieg tube (hence increasing M_3), or through use of a double expansion nozzle as shown on the lower sketch of Fig. 1. In the latter case the supply flow enters a plenum, expands to supersonic Mach number through a first stage nozzle (shown as an orifice plate), passes through a shock region, and finally expands to the test section. The total pressure of the flow is reduced by the shock system, and mass continuity requires that the area of the second throat be increased over the first throat in direct proportion to the total pressure ratio. The double nozzle thus exchanges supply pressure for test section scale. This capability has been found useful for pulsed gasdynamic lasers[7] and has a similar direct application to aerodynamic testing. The increased amount of supply gas required to maintain Re capability is a basic cost of increased scale; the increased pressure level is the major additional cost of the double expansion nozzle. Two new aerodynamic concerns arise in the double expansion nozzle: these are the time for the nozzle flow to reach a steady condition, and the possibility of test flow disturbances originated at the orifice plate. These questions are taken up in the section dealing with nozzle aerodynamics.

Supply Tube

Analysis of Core Flow Variations

A small perturbation analysis of the flow in a supply tube has been carried out, following the general procedure of Demyanov[8] and Spence and Woods.[9] A long slender pipe is considered with coordinates and notation as shown on Fig. 3. The constraint $L/d \gg 1$ allows neglect of radial velocity components, while $M_3 \ll 1$ keeps the expansion wave thickness small so that the flow within it can be neglected. Cross-sectional area perturbations ($\approx 2\Delta d/d$) and initial temperature variations ($\Delta T_4/T_4$) are also kept small. The nonsteady continuity equation can then be written in cylindrical coordinates, integrated across the duct, and expanded for small values of δ^*/d, yielding

$$\frac{\partial}{\partial t}\rho_e + \frac{\partial}{\partial x}(\rho_e u_e) \approx \frac{4}{d}\frac{d}{ds}[\rho_e(U-u_e)\delta_s{}^*] - \frac{2}{d}\rho_e u_e \frac{dd}{dx} \quad (1)$$

for the core flow. Here U is a single speed assigned to the expansion wave and $s = Ut - x$. The right-hand side of Eq. (1)

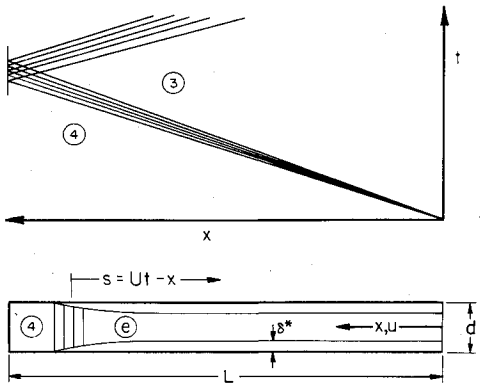

Fig. 3 Wave diagram and schematic for analysis of supply tube flow.

contains the boundary layer and area variation effects, which appear as mass addition terms to the one-dimensional nonsteady continuity equation for the core flow. Conservation of momentum in the core flow can be written

$$\rho_e[(\partial u_e/\partial t)+u_e(\partial u_e/\partial x)]+(\partial p_e/\partial x)=0 \tag{2}$$

while the condition of particle isentropy of an ideal gas is

$$[(\partial/\partial t)+u_e(\partial/\partial x)]\ln(p_e/\rho_e)=0 \tag{3}$$

Equations (1–3) can be linearized for small perturbations of the various flow variables from condition 3, the unperturbed state. Assuming a $\frac{1}{7}$th power velocity profile, δ^*/d can be written in terms of $(s/d)^{4/5}$ multiplied by a constant that is dependent on the values of M_3 and p_4d (see Fig. 2). This can be combined with the linearized equations to yield two ordinary differential equations in two characteristic independent variables. The equations are easily integrated, with functions of integration that must be evaluated by application of boundary conditions at both ends of the column of gas. A fixed area sonic throat is assumed to exist downstream of the open end, allowing the Mach number at the pipe exit to be related to the changing area ratio caused by the pipe boundary-layer growth. The expansion wave is treated as an isentropic "expansion shock" at the other end. This relates the perturbations to each other and allows determination of U as a function of M_3 and the initial conditions.

The analysis yields closed form expressions for the fluid properties in the core flow as a function of time and position along the tube. When plotted versus x at a fixed t, the pressure shows a positive perturbation immediately behind the expansion wave. This is caused by the deceleration and weakening of the wave. The peak decreases to become a negative perturbation at the pipe exit, caused in part by the boundary condition requirement that M_e increase. When evaluated at the pipe exit, the pressure and velocity perturbations reduce to

$$\frac{1}{2\gamma M_3}\frac{\Delta p_3}{p_3}=-\left.\frac{\delta^*}{d}\right|_{s/d=a_4t/d}+\left.\left[\frac{\Delta d}{d}+\frac{1}{4}\frac{\Delta T_4}{T_4}\right]\right|_{x/d=a_4t/2d}-\left.\frac{1}{2}\frac{\Delta T_4}{T_4}\right|_{x/d=M_3a_4t/d}$$

and (4)

$$\frac{\Delta u_3}{u_3}=4\left.\frac{\delta^*}{d}\right|_{s/d=a_4t/d}+(\gamma-1)M_3\left.\left[\frac{\Delta d}{d}+\frac{1}{4}\frac{\Delta T_4}{T_4}\right]\right|_{x/d=a_4t/2d}+\left.\frac{\Delta T_4}{T_4}\right|_{x/d=M_3a_4t/d}$$

where terms of order M_3 have been neglected compared with unity (resulting in $U\approx a_4$). The boundary-layer contributions to Eqs. (4) may be evaluated using Fig. 2. The last terms on the right hand side of Eqs. (4) are due to entropy changes caused by initial temperature variations. Both ΔT_4 and Δd are measured with respect to the open end. As a consequence of the linearization of the equations of motion, these variations are seen to contribute separate superimposable terms arising from specific locations along the pipe. Details of the mathematical development of Eqs. (4) will be reported at a later time, together with a discussion of the high M_3 (thick expansion wave) case and the case of flow with large perturbations (large L/d).

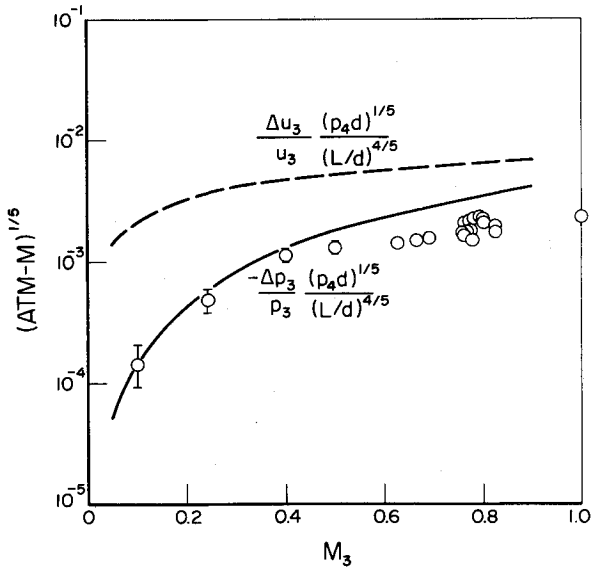

Fig. 4 Boundary layer induced perturbations in the core flow.

Results and Comparison with Experiment

Figure 4 is a plot of the perturbations in the core flow due to only the boundary-layer terms of Eqs. (4). The curves are for $T_4 = 300°K$ nitrogen and are evaluated when the test period is just over and the perturbations are a maximum. For this δ^*/d was obtained from Becker's model of Fig. 2 with $s = 2L$. The lower curve of Fig. 4 shows that significant pressure perturbations can occur, particularly as M_3 increases. It is also seen that $\Delta u_3/u_3$ is generally larger than $\Delta p_3/p_3$. Consistent with the low M_3 limit of applicability of the theory $(\Delta p_o/p_o)_3$ equals $\Delta p_3/p_3$. Further, $(\Delta T_o/T_o)_3$ is given by $(\gamma-1)/\gamma$ times $\Delta p_3/p_3$ as the core flow is taken to be isentropic in the absence of initial T_4 variations. Although Becker's results[6] are not presented in as simple a form as Fig. 4, specific comparisons are in approximate agreement at low M_3.

Experiments have been carried out in order to check the analysis and its extrapolation to high M_3 and large perturbations. For this purpose, static pressure time histories were taken at the open end of 2.5 cm i.d. supply pipes, using quartz pressure transducers. M_3 was varied through the use of choke plates

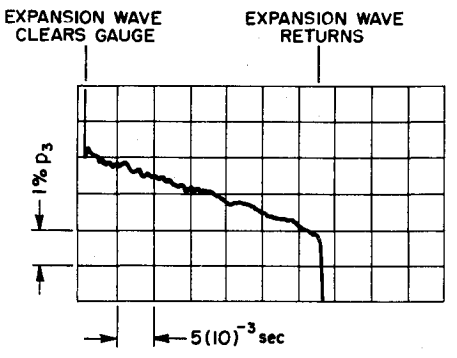

Fig. 5 Pressure history at exit of supply tube.

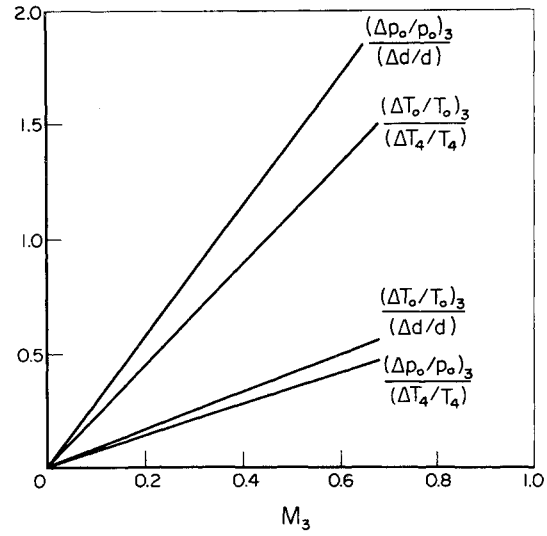

Fig. 6 Effects of tube cross-sectional area and initial temperature variations.

located just downstream of the gage and upstream from the starting diaphragm. The sample trace of Fig. 5 was obtained using a nitrogen charge of 60 atm. at 300°K, with $M_3 = 0.1$ and $L/d = 250$. The expansion wave clears the gage in the first millisecond, dropping the pressure to the nominal p_3 value. The expanded vertical scale of the trace then shows the pressure decline with time until the expansion wave returns. The decline is nearly linear, in approximate agreement with the $t^{4/5}$ dependence predicted by Eqs. (4) coupled with Fig. 2. Similar measurements were made at different M_3 and the results are collected on Fig. 4. The circular symbols are for individual runs, while the bars on some symbols represent the extreme limits of the results of at least ten separate experiments at fixed M_3. The strong M_3 dependence and the use of L/d of 250 and 500 gave actual $\Delta p_3/p_3$ values ranging from 1–20%.

No systematic dependence on perturbation level was detected in the experiments. The agreement between the measured and calculated values for $\Delta p_3/p_3$ is seen to be excellent at low M_3. At high M_3 the agreement is still remarkably good. An improved boundary-layer model would help to close the gap between theory and experiment. The assumptions in both models on Fig. 2 are incorrect at large M_3, and the $\frac{1}{7}$th power velocity profile is known to be inaccurate at large Re. To be consistent however, high M_3 refinements of the analysis must also involve abandonment of the expansion shock concept and inclusion of the throat boundary layer in the open end boundary condition (i.e., see next section).

Care had to be taken to insure that cross-sectional area and initial temperature variations did not compete with the viscous effects in the experiments. Further, thin-film heat-transfer gage measurements showed that small axial temperature gradients can be set up in the supply gas due to compression heating during the charging process. The expected sensitivity to these effects is shown on Fig. 6. The figure gives the open end flow perturbations at the end of the run time ($a_4 t = 2L$) in unheated nitrogen. The area and temperature terms of Eqs. (4) were considered separately, assuming small $\Delta d/d$ and $\Delta T_4/T_4$ at the closed end measured with respect to the open end. A linear variation in $\Delta T_4/T_4$ was also assumed. Because the pipe exit Mach number is constant in the absence of viscous effects, $(\Delta p_o/p_o)_3$ and $(\Delta T_o/T_o)_3$ at the open end are again identical to $\Delta p_3/p_3$ and $\Delta T_3/T_3$, respectively.

The normalized flow perturbations of Fig. 6 are seen to be generally similar in magnitude to the normalized axial perturbation causing the variation. There is a linear increase with M_3, which can be shown to lead to an overestimation of the flow disturbance at high M_3. Although a systematic experimental study of these effects was not undertaken, a few experiments established that the predicted magnitudes are of the right general order. When used with measurements of the variations in d and T_4, Fig. 6 showed that contributions from nonviscous effects could generally be neglected for the experiments of Fig. 4. This may not be true for a large facility where high levels of cross-sectional area and temperature uniformity may be difficult to maintain.

Coupling to the Nozzle

Nozzle Inlet Contraction

The core flow perturbations just discussed will ultimately appear in the downstream test flow. To these must be added any flow perturbations caused by the feeding of the pipe boundary layer into the nozzle. The desirability of nozzles with large dimension (see Introduction) leads to the use of high M_3 and consequent low pipe-to-throat area ratios. As this inlet contraction is reduced the thick pipe boundary layer begins to affect the development of the nozzle boundary layer. The effective area ratio for the test section of the nozzle can thus become time dependent, with a resultant time dependence for the test flow variables.

The effect has been explored using an integral type of steady turbulent analysis[10] to calculate the boundary layer along the walls of a set of specified nozzles. The results, using various input values of δ^*/d (Fig. 2), are shown on Fig. 7. Here $(A/A^*)_{\text{eff}}$ is the test-section-to-throat area ratio with boundary-layer correction, whereas (A/A^*) is the geometric area ratio with no corrections. The relative change is plotted versus δ^*/d for representative nozzles with nominal test Mach numbers of 0.5, 1, and 3. Selected values of M_3 were 0.1, 0.5, and 1.0 corresponding to inlet contraction area ratios of 6, 1.3, and 1, respectively. The nozzles were chosen to be two dimensional, having subsonic convergence made with two tangentially-joined arc sections. The $M = 0.5$ and 1 nozzles had throat locations three test-section-heights downstream from the assumed test section location at the end of the inlet contraction. The supersonic portion of the $M = 3$ nozzle was also approximately three test-section-heights long, with the external flow for the boundary-layer program obtained from method-of-characteristics calculations. The calculated two-dimensional value of the area change parameter has been doubled in order to include a representative contribution from the flat nozzle walls. There is a weak dependence on pressure level, varying from $(p_o d)^{-1/5}$ at low values of δ^*/d to

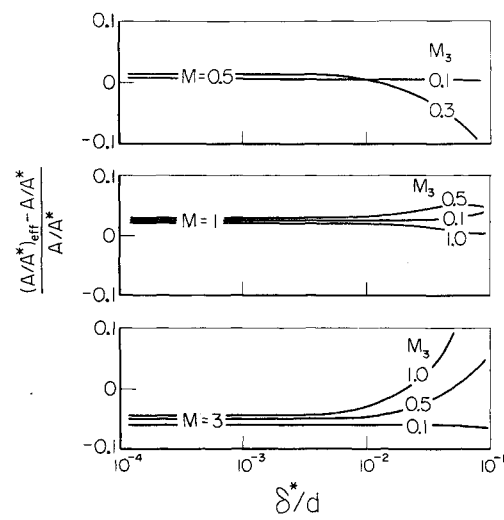

Fig. 7 Influence of tube boundary layer on effective nozzle test section area ratio.

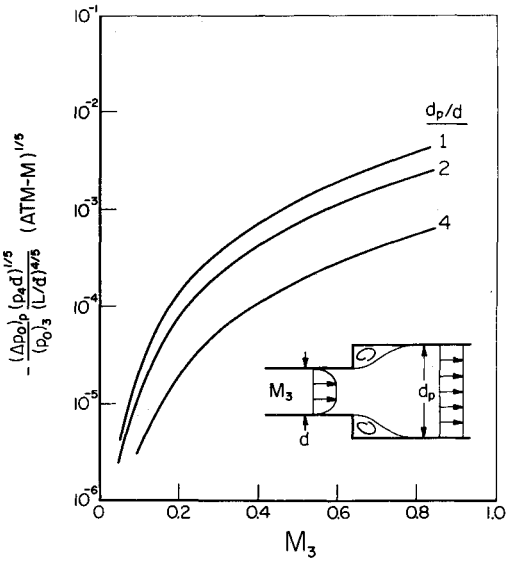

Fig. 8 Total pressure loss due to mixing.

complete independence at high values. Figure 7 was prepared for nitrogen with $T_o = 300°K$ and $p_o d = 0.5$ atm-m.

The effective area change parameter has a finite value at small δ^*/d that is determined by the normal steady boundary-layer correction. As time progresses and δ^*/d thickens, the effective area change can become quite pronounced. While Fig. 7 shows that a $M_3 = 0.1$ subsonic contraction is sufficient to effectively isolate the nozzle boundary layer from that in the pipe, this is clearly not true for higher M_3. The perturbations could be particularly troublesome near $M = 1$ where a small area change causes a large variation in the test flow. For this M, the figure suggests that there is also a moderate M_3 value (between 0.5 and 1) that will minimize the effect.

Mixing in a Plenum

A reservoir may be used upstream of the nozzle inlet to slow and mix the core and boundary-layer flow emerging from the pipe. Some Ludwieg tubes are designed with such a plenum, and the region upstream of the orifice plate in a double expansion nozzle (Fig. 1) would be expected to serve this purpose. In order to find the maximum p_o losses that will occur assuming complete mixing, statements of conservation of mass, momentum, and energy may be written across the mixing region. For axial symmetry these become

$$\rho_3 u_3(1-4\delta^*/d) = \rho_p u_p(d_p/d)^2$$
$$\rho_3 u_3{}^2(1-4\delta^*/d-4\theta/d)+p_3(d_p/d)^2 = (\rho_p u_p{}^2+p_p)(d_p/d)^2 \quad (5)$$
$$\text{and} \quad (\rho u T_o)_3(1-4\delta^*/d+4\varepsilon/d) = (\rho u T_o)_p(d_p/d)^2$$

to first order in the various boundary thicknesses. Equations (5) assume that there is no appreciable wall shear during the mixing and that any diameter change occurs with p_3 acting over the upstream face of the expansion. It is necessary to relate the various boundary-layer thicknesses in order to proceed. Using the simple Becker model[5] and neglecting terms of order $(\delta^*/d)^2$ and $(M_3{}^2)^2$, there can be obtained from the algebraic solution of Eqs. (5)

$$(p_o)_p/(p_o)_3 = 1-(28/9)\gamma M_3{}^2(\delta^*/d) \quad \text{for} \quad d_p = d$$
$$(p_o)_p/(p_o)_3 = 1-\gamma M_3{}^2[\tfrac{1}{2}-(d/d_p)^2+(64/9)(d/d_p)^2(\delta^*/d)] \quad \text{for} \quad d_p{}^2 \gg d^2 \quad (6)$$

while

$$(T_o)_p/(T_o)_3 = 1-(28/5)(\gamma-1)(M_3{}^2/2)(\delta^*/d)$$

and is independent of the diameter ratio. Terms of order $M_3{}^2(d/d_p)^4$ were neglected in the development of the second simplified expression for $(p_o)_p/(p_o)_3$. Such terms do not appear when d_p is set equal to d in Eqs. (5), so that the first of Eqs. (6) is more accurate for this case.

The pressure perturbations from Eqs. (6) were coupled with the Becker curve on Fig. 2 and plotted versus M_3 on Fig. 8. For $d_p = d$, $(\Delta p_o)_p/(p_o)_3$ is strongly dependent on M_3 and goes to zero with δ^*/d as would be expected. When $d_p > d$ a separation loss automatically results from the equations regardless of the value of δ^*/d. This loss is predicted by the first two terms on the right side of the second expression of Eqs. (6), and is maximized by the choice of p_3 acting on the initial expanded cross section. The remaining term gives the loss due to δ^*/d and it is this which is exhibited as the $d_p > d$ curves of Fig. 8. These curves show less loss than the $d_p = d$ curve, which itself predicts a somewhat smaller loss than that in the core flow (Fig. 4). The curves of Fig. 8 were found to agree within 10% with exact solutions of both Eqs. (5) and conservation equations containing second order boundary-layer terms. Experimental results (i.e. Fig. 9) agreed with Fig. 8 in that mixing pressure losses were predicted and found to be too small ($<\frac{1}{2}\%$) to be distinguished for the conditions of the runs. As with Fig. 4 however, the mixing losses can become significant at large M_3 and L/d.

The total temperature change of Eqs. (6) is negative. It is actually expected to be positive due to heat transfer into the Ludwieg tube flow. An accurate prediction of $(T_o)_p/(T_o)_3$ would require incorporation of this effect through a nonconstant boundary-layer density profile.

Nozzle

Starting Process

The starting times of various nozzle-and-diaphragm configurations can be calculated by the method of characteristics. It is generally found that nozzles with upstream diaphragms start faster, but that downstream diaphragm starts are still quite short compared with the available test time. The problem is most severe at transonic Mach numbers, but even here it is not a serious limitation, consuming less than 10% of the available test time from a $L/d = 100$ supply pipe.[2]

A simple model has been developed for predicting the starting time of the between-stage volume (V) of a double expansion nozzle (see Fig. 1) with an upstream diaphragm. This model ignores the wave processes entirely and treats the starting process as a mass filling problem. At low initial pressures an initial shock wave quickly traverses V and reflects, setting up a sonic outflow through the downstream throat (A^*). Optical studies have shown that part of this wave moves back upstream to eventually form the stationary throttling shock in the exit flow from the orifice plate. The upstream and downstream throats may thus be regarded as choked at essentially the beginning of the starting process. The difference between the rate of outflow and the constant rate of inflow can then be set equal to the rate of mass accumulation within V, using a mean value of p within V at any instant of time. For adiabatic flow of a perfect gas, the solution to the differential equation can be written in the form

$$p_o/(p_o)_p = A_{op}{}^*/A^*\{1-\exp[-(\gamma+1)a_o A^* t/2V]\}^{-(\gamma+1)/2(\gamma-1)} \quad (7)$$

Steady state is reached when the total pressure ratio $= A_{op}{}^*/A^*$. From Eq. (7), p_o has reached 90% of its final value when

$$t \approx 4V/(a_o A^*) \quad (8)$$

while twice this time corresponds to a p_o within 1% of final value. Note that the starting time is independent of the upstream (orifice plate) throat area, which makes its appearance in the pressure level finally achieved [Eq. (7)].

Pressure histories taken with small double expansion nozzles are in agreement with Eqs. (7) and (8). Figure 9 was obtained with a quartz pressure gage mounted in the wall of the between-stage volume of an $A_{op}{}^*/A^* = 0.1$ double expansion nozzle. The

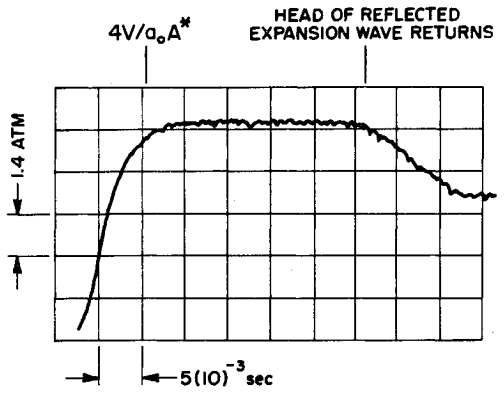

Fig. 9 Pressure history between stages in double expansion nozzle.

nozzle was driven by 6.6 m of 2.5 cm i.d. supply operating at $M_3 = 0.26$ with nitrogen at $T_4 = 300°K$. The geometry was similar to that of the lower sketch on Fig. 1. The Mach number at the gage station was low (≈ 0.15) so that the static and total pressures are very nearly identical. The pressure is seen to rise from the prerun evacuated value of essentially zero, level off, and then finally decline as the reflected wave appears at the gage station. The calculated 90% rise time and the calculated run time are shown on the figure. They are seen to be in good agreement with the experimental results. The plateau pressure level was within $\pm 5\%$ of the ideal value, the uncertainty being due to difficulties in measuring absolute pressures and to inaccuracies in $A_{op}{}^*$ when fine orifices are involved. Small reductions in total pressure level due to separation [Eq. (6)] and due to the orifice boundary layers could not be resolved. The pressure perturbations of Figs. 4 and 7 together amounted to less than a 1% fall over the useful run time for this experiment, also in agreement with Fig. 9.

A faster start might be expected if the initial pressure in V were raised, however individual waves then become important and the validity of the simple model questionable. Experiments indicate that the starting time is not strongly sensitive to the initial pressure level.

Flow Quality

Nozzles designed to produce large scale flows will use the least inlet convergence (highest M_3) consistent with maintaining acceptable flow quality. Because of the generally high Re, nozzle boundary-layer corrections will be small if the tube δ^* effects are controlled (see Fig. 7). Thus integral methods of correcting the nozzle wall should be adequate. There will be some uncertainties due to transition and the corner flow of two-dimensional nozzles, with the usual problems caused by close nozzle and model coupling in transonic flow.

There are unique flow quality problems that could arise from the first stage in the double expansion nozzle. Use of a single first stage nozzle would add to V and the starting time [Eq. (8)], and need a bleed in order to avoid nonuniformities caused by the interaction between the nozzle boundary layer and the throttling shock. Orifice plates (see Fig. 1) provide a simple and flexible alternative. Interferograms of the flow in a small $M = 3$ nozzle equipped with such plates have shown virtually no difference between a double expansion and conventional Ludwieg tube drive. However, the possibility of small scale orifice-plate-generated turbulence in the test flow needs to be explored further.

The limiting case of incompressible flow downstream of low blockage wire grids has been extensively studied[11] because of its fundamental importance to understanding homogeneous turbulence. It has been found that grid generated vorticity quickly becomes isotropic, after which the geometry of the grid is important only in assigning an effective origin and an initial scale size to the resultant motion. Two distinct regimes have been identified in the decay process. In the first eddies can only interact inertially as there is insufficient time for significant viscous losses. This inertial interaction breaks down the large eddies and creates a spectrum of eddy size in the flow. The equations of motion suggest that the fluctuating kinetic energy should depend on the inverse of the downstream distance and the experimental evidence verifies this decay law. The fluctuation energy becomes concentrated in smaller eddies as the downstream distance increases, with viscous dissipation eventually becoming the dominant mechanism for decay. The location of this point is Re dependent, but it will usually occur at turbulence levels well below present interest.

Corrsin[12] has measured the effect of grid geometry and blockage on initial scale size for incompressible flow. The scale size was found to change from a value equivalent to the wire spacing for low blockage grids to order-of-magnitude larger values at high blockage. In the latter case, the evidence suggests that many individual jets move in a collective fashion, creating large initial eddies and a correspondingly slow decay. Such motion arises from an instability involving the whole flowfield in the vicinity of the grid. In extrapolating these results to high speed flow, it is useful to note that although increases in u result in less eddy transport time to a given downstream station, the eddies rotate proportionately faster. Thus, direct effects of u should cancel out. Further, compressibility effects should not be large for moderate M, and will in fact be overshadowed by uncertainties in the scale size.

Figure 10 presents hot wire measurements taken 15–150 cm downstream of orifice plates mounted in a 5-cm-i.d. pipe attached to a draw down wind tunnel. The orifice plates used for these experiments had 90% geometric blockage with either 1000-$\frac{1}{2}$ mm holes, 240-1 mm holes, or 60-2 mm holes. The pipe was equipped with downstream chokes to control the duct Mach number (here set at 0.2) and hence also the strength of the throttling shock system imbedded in the plate exit flow. Only those data which were clearly not affected by the pipe wall boundary layer are shown on Fig. 10. Here the ordinate is the mean downstream speed divided by the *rms* velocity fluctuation. It is plotted versus the downstream distance measured in units of the orifice hole spacing (D). Each collection of data shows the expected linear dependence of $(u/u_{rms})^2$ on x/D, with a similar effective origin for the turbulence. A few points (indicated by filled-in symbols) were taken with the orifice plate replaced by ordinary window screening. These results are seen to be in agreement

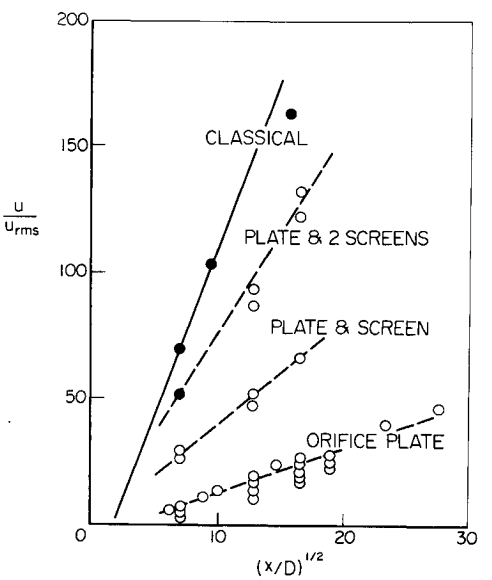

Fig. 10 Turbulence decay downstream of high blockage orifice plates.

with the classical low speed measurements[11] which show that $(u/u_{rms})^2 \approx 100\ x/D$. The high blockage orifice plates produced a decay that was found to be independent of D and detailed orifice plate geometry, but required two orders-of-magnitude more distance to achieve the same turbulence reduction. A similar general behavior was observed for both higher (0.46) and lower (0.04) pipe Mach numbers. Figure 10 shows that mounting a single 100-mesh screen immediately downstream increased the decay rate, while addition of a second screen (2 cm further downstream) brought the rate nearly to the classical value. The screens appear to stabilize the flow, controlling cooperative jet motion and reducing the initial scale size. There will be a further direct increase in u/u_{rms} as u is increased through the main nozzle.[11] Both effects are important to the design of double expansion nozzles.

Conclusions

A linearized theory has been developed for the flow nonuniformities caused by the growing turbulent boundary layer in a Ludwieg tube supply. The theory predicts a maximum open-end pressure perturbation climb of over an order-of-magnitude from its value at $M_3 = 0.1$ to $2(10)^{-3}(L/d)^{4/5}(p_4 d)^{-1/5}$(atm-m)$^{1/5}$ at $M_3 = 0.5$. Pressure measurements were found to be in good agreement at low M_3, diverging slightly at high M_3 due to inherent limitations in the analysis. A direct dependence on M_3 was predicted for the effects of pipe cross-sectional area and initial temperature nonuniformity, with percent flow perturbations generally of the order of the percent nonuniformity causing them.

Calculations for a representative series of nozzles showed that growth of the pipe exit δ^*/d to greater than 1% can affect the nozzle boundary layer. The resulting nonsteady change in the effective nozzle area ratio becomes pronounced as M_3 is raised. A linearized analysis was used to calculate the limiting case of complete mixing of the pipe exit boundary layer and core flow in a nozzle plenum. A total pressure loss dependent on $M_3{}^2$ and the plenum-to-pipe area ratio resulted, with a magnitude at $M_3 = 0.5$ that can be as large as one-half that predicted for the core flow alone.

The aerodynamic perturbations just summarized all originate in the long supply pipe of a Ludwieg tube. They are superimposable in their linearized form. Although often small, they provide the ultimate limit on temporal flow quality, becoming particularly significant for large M_3 and L/d. The double expansion nozzle offers an alternative to the use of increased M_3, and is a promising way to achieve large dimension test flows. Experiments showed that these nozzles start quickly, in agreement with the predictions of a simple mass filling model. Further, hot wire measurements of orifice-plate-generated turbulence established the possibility of achieving the rapid classical decay, $(u/u_{rms})^2 \approx 100\ x/D$. There will be an additional reduction in turbulence for accelerating nozzle flows. It is concluded that aerodynamic concerns will not limit application of the double expansion nozzle.

References

[1] Ludwieg, H., "Der Rohrwindkanal," *Zeitschrift für Flugwissenschaften*, Vol. 3, No. 7, July 1955, pp. 206–216.

[2] Enkenhus, K. R. and Merritt, D. L., "Evaluation of Two Types of Facilities to Fulfill the Need for High Reynolds Number Transonic Testing," NOLTR 71-147, July 1971, Naval Ordnance Lab., White Oak, Silver Spring, Md.

[3] Whitfield, J. D., Schueler, C. J., and Starr, R. F., "High Reynolds Number Transonic Wind Tunnels-Blowdown or Ludwieg Tube?," *Facilities and Techniques for Aerodynamic Testing at Transonic Speeds and High Reynolds Number*, AGARD-CP-83-71, 1971.

[4] Mirels, H., "Boundary Layer Behind Shock or Thin Expansion Waves Moving into Stationary Fluid," TN 3712, 1956, NACA.

[5] Becker, E., "Unsteady Boundary Layer Behind Compression Shocks and Expansion Waves," *Progress in Aeronautical Sciences*, Vol. 1, 1961, pp. 104–173.

[6] Becker, E., "Reibungswirkungen beim Rohrwindkanal," Mitt. aus dem Max-Planck-Institut fuer Stroemungsforschung u.d. Aerodynamischen Versuchsanstalt, No. 20, 1958.

[7] Russell, D. A., Christiansen, W. H., and Hertzberg, A., "Shock Tube Lasers," *Shock Tube Research: Proceedings of the VIIIth International Shock Tube Symposium*, edited by Stollery, Gaydon, and Owen, Chapman and Hall, London, 1971, pp. 45A/1–12.

[8] Demyanov, Yu A., "The Influence of the Boundary Layer on the Character of the Flow of Gas in a Tube Behind a Moving Shock Wave," *Prikladnaia Matematika i Mekhanika*, Vol. 21, No. 4, 1957, pp. 473–477; also Translation 796, 1959, R.A.E. Library.

[9] Spence, D. A. and Woods, B. A., "Boundary Layer and Combustion Effects in Shock Tube Flows," *Colston Papers*, Vol. XI, *Proceedings of the Eleventh Symposium of the Colston Research Society*, Butterworths, London, April 1959.

[10] Sasman, P. K. and Cresci, R. J., "Compressible Turbulent Boundary Layer with Pressure Gradient and Heat Transfer," *AIAA Journal*, Vol. 4, No. 1, Jan. 1966, pp. 19–25.

[11] Batchelor, G. K., *The Theory of Homogeneous Turbulence*, Cambridge University Press, Cambridge, Mass., 1967, pp. 68–75, 133–139.

[12] Corrsin, S., "Turbulence: Experimental Methods," *Handbuch der Physik*, Vol. VIII/2, edited by S. Flügge, Berlin, 1963, pp. 524–590.